journal

J. Am. Ceram. Soc., 91 [3] 996–1001 (2008)
DOI: 10.1111/j.1551-2916.2007.02226.x
© 2008 The American Ceramic Society

Interface Character Distributions in WC–Co Composites

Chang-Soo Kim,[*,‡,¶] Ted R. Massa,[§] and Gregory S. Rohrer[*,†,‡]

[‡]Department of Materials Science and Engineering, Carnegie Mellon University, Pittsburgh, Pennsylvania 15213

[§]Corporate Technology, Kennametal Incorporated, Latrobe, Pennsylvania 15650

The geometric and crystallographic characteristics of interfaces in WC–Co composites with a range of grain sizes and carbide volume fractions have been comprehensively characterized. The carbide crystals are most frequently terminated by (0001) and $(10\bar{1}0)$ surfaces. The average number of carbide vertices per grain and the basal-to-prismatic face area ratio of the WC–Co interfaces increase with the carbide volume fraction. The three most frequently occurring WC/WC grain boundaries are 90° twist boundaries about $[10\bar{1}0]$, 30° twist boundaries about [0001], and asymmetric 90° boundaries about $[\bar{2}110]$. The boundary populations do not vary with grain size or carbide volume fraction, suggesting that they are determined by the grain boundary energy anisotropy.

I. Introduction

Tungsten Carbide-Cobalt composites are used in a range of applications where hardness and abrasion resistance are important. It is well known that the properties of these materials can be correlated to certain microstructural metrics. For example, hardness increases as carbide volume fraction increases and as mean grain size decreases. The toughness of the composites follows the opposite trends.[1–3] In metals with the face-centered cubic (FCC) crystal structure, macroscopic properties have been closely linked to the grain boundary character distribution (GBCD).[4] The most important feature in the GBCD of FCC metals is the concentration of Σ3 boundaries that are special with respect to their geometry and low energy. Improvements in mechanical properties are generally correlated to increases in the fraction of Σ3 boundaries. It has recently been reported that WC–Co composites contain relatively high concentrations of WC grain boundaries that are special with respect to their geometry and energy.[5–9] Of particular prominence are pure twist grain boundaries with 90° rotations about $[10\bar{1}0]$, which are sometimes referred to as Σ2 boundaries. By analogy to the FCC metals, it might be possible that these boundaries are beneficial to the mechanical properties of WC–Co composites. However, it is not yet known how the concentration of these boundaries varies with microstructural characteristics or whether their properties can be correlated to the properties of WC-containing materials. Therefore, the goal of this paper is to determine whether the population of special boundaries in WC–Co composites is sensitive to changes in grain size or carbide volume fraction.

To address this question, the geometry and crystallography of the interfaces in seven different WC–Co composites with a range of grain sizes (1.4–5.3 μm) and carbide volume fractions (0.69–0.88) have been comprehensively characterized. Preliminary results for two of the specimens (labeled A and E in Table I) were reported earlier, and the current paper extends and completes the analysis of these microstructures and compares them with five additional materials so that the trends can be determined with grain size and Co volume fraction.[6] In the past, GBCDs of single-phase polycrystals have been derived from extensive orientation maps of polycrystals.[10] Here, these techniques are adapted for the study of composite microstructures so that the distributions of WC/Co and WC/WC interfaces can be analyzed separately. Throughout the analysis, only the WC orientations are considered. In addition to interface character distributions, the analysis allows the measurement of grain size distributions, phase contiguity, and shape parameters such as the average number of vertices and the aspect ratio. The results show that all the samples examined have significant numbers of special interfaces. The fraction of geometrically special WC grain boundaries is remarkably constant with grain size and carbide volume fraction, suggesting that a scale-invariant steady state is reached during grain growth. The distribution of WC/Co interfaces, on the other hand, changes systematically with carbide volume fraction.

II. Experimental Procedure

(1) Materials

The microstructures of seven WC–Co samples with different grain sizes ranging from 1.4 to 5.3 μm and WC volume fractions ranging from 0.69 to 0.88 were characterized. WC is hexagonal with lattice constants $a = 2.91$ Å and $c = 2.84$ Å. If there is sufficient C and W dissolved in the Co, the cubic FCC phase is stabilized. However, at lower solute contents, the FCC ($a = 3.56$ Å) and hexagonal close packed (HCP) ($a = 2.52$ Å and $c = 4.10$ Å) phases occur simultaneously.[11] The samples were consolidated via liquid-phase sintering for approximately 45 min at temperatures in the range of 1400°–1600°C. Materials with the highest Co binder fractions were sintered at the lower end of this temperature range and those with the least binder were sintered at the higher temperature. The composites have no intentionally added alloying elements and are referred to as straight grades. The grain sizes and carbide volume fractions for each specimen grade are listed in Table I. Samples were prepared for microscopic analysis by polishing with a diamond abrasive and then etching in Murakami's reagent (10 g potassium ferricyanide+10 g sodium hydroxide+100 ml distilled water) for 1 min. The reagent preferentially attacks the carbide phase with different rates and produces topographic differences at the binder/carbide interfaces and the carbide/carbide boundaries that lead to sharp contrast in atomic force microscopy (AFM) images. This preparation also yields WC surfaces suitable for electron backscatter diffraction (EBSD) mapping.

(2) AFM imaging

Some of the geometric data were determined from micrographs recorded using a Park Scientific Instruments Cp or a Thermomicroscopes M5 AFM. Gold-coated, sharpened pyramidal Si_3N_4 probes (Thermomicroscopes ML06A-F, Sunnyvale, CA) were operated in contact mode. The field of view for each AFM

R. Hay—contributing editor

Manuscript No. 23545. Received August 2, 2007; approved November 9, 2007.
This work was supported primarily by Kennametal Incorporated and the Pennsylvania DCED. Partial support by the MRSEC program of the National Science Foundation under Award Number DMR-0520425 is also acknowledged.

[*]Member, The American Ceramic Society.
[†]Author to whom correspondence should be addressed. e-mail: gr20@andrew.cmu.edu
[¶]Current address: Division of Chemistry and Materials Science, U.S. Food and Drug Administration, Silver Spring, MD 20993, USA.

Table I. Summary of Microstructural Data for WC–Co Composites

Sample	Grain diameter (std), L, μm	Intercept length (std), L^*, μm	WC volume fraction	Contiguity	Vertices (std)	Aspect ratio man/auto
A	5.31 (3.19)	5.25 (3.89)	0.88	0.595	6.94 (3.15)	1.52 1.59
B	1.65 (0.97)	1.58 (1.20)	0.88	0.591	6.87 (2.55)	1.50 1.55
C	1.41 (0.90)	1.44 (1.06)	0.82	0.501	6.78 (3.25)	1.38
D	1.53 (0.83)	1.43 (1.02)	0.82	0.500	6.45 (2.35)	1.33 1.38
E	1.40 (0.88)	1.41 (1.12)	0.69	0.351	6.16 (2.89)	1.18 1.16
F	3.12 (1.80)	2.94 (2.10)	0.83	0.521	6.69 (3.28)	1.47
G	2.59 (1.89)	2.59 (1.89)	0.85	0.551	6.75 (2.59)	1.43 1.50

image was selected based on a rough estimate of WC grain size (60 μm × 60 μm for A, 20 μm × 20 μm for B–E, and 40 μm × 40 μm for F and G), such that each AFM section contains 100–180 carbide grains. The microscope was programmed to automatically record 100 images in a 10 by 10 array such that there was approximately a 10% overlap with adjacent images in the array. Thus, the total scanned areas ranged from 540 μm × 540 μm for sample A to 180 μm × 180 μm for samples B–E and 360 μm × 360 μm for samples F and G. This imaging procedure allows the shapes of many grains to be determined with high resolution. There are 512 × 512 pixels in each of the AFM images, so the pixel spacing is 0.12 μm (A), 0.04 μm (B–E), and 0.08 μm (F and G), and this means that there were more than 32 pixels per average grain diameter. A typical AFM image of a WC–Co composite is illustrated in Fig. 1(a). The individual WC grains are dissolved at different rates by the etching solution and, therefore, have various shades of darker contrast. The differential etching allows both WC/Co and WC/WC boundaries to be easily identified.

(3) Geometric Analysis

The interface positions in the AFM images are digitized using a program that automatically records the vector components of binder/carbide (l_{bc}) and carbide/carbide (l_{cc}) line segments when the user traces them with a computer mouse. Hence, polygonal closed contours of WC particles consisting of l_{bc} and l_{cc} line segments joined at N vertices can be constructed. For each of the seven specimen grades, the boundaries in 20 AFM images were skeletonized so that, for each grade, the geometric results are based on measurements of approximately 2500 carbide grains. An example of a skeletonized map is shown in Fig. 1(b). The grain area (A) of carbide is then computed as the total number of pixels within a closed polygon, multiplied by the area per pixel. Grain diameters (d) are computed by assuming that the grain area is circular ($d = 2(A/\pi)^{1/2}$). The contiguity of carbide phase (C) is computed according to the following expression:

$$C = \frac{2\sum_i l_{cc}^i}{\sum_{i,j}(2l_{cc}^i + l_{bc}^j)} \tag{1}$$

where l_{cc} is the length of a carbide/carbide grain boundary and l_{bc} is the length of a binder/carbide interface. For comparison, we also examined the carbide grain size determined from linear-intercept lengths. Using all 512 lines, in the two perpendicular directions, and in each of the 20 skeletonized AFM images as test lines, there were approximately 2×10^4 test lines for each specimen grade. From these test lines, we determined the mean carbide intercept length, L, and the mean binder intercept length, λ, and the average number of intercepts per unit length of test line with carbide/carbide boundaries (N_{cc}) and binder/carbide interfaces (N_{bc}). The stereologically determined carbide

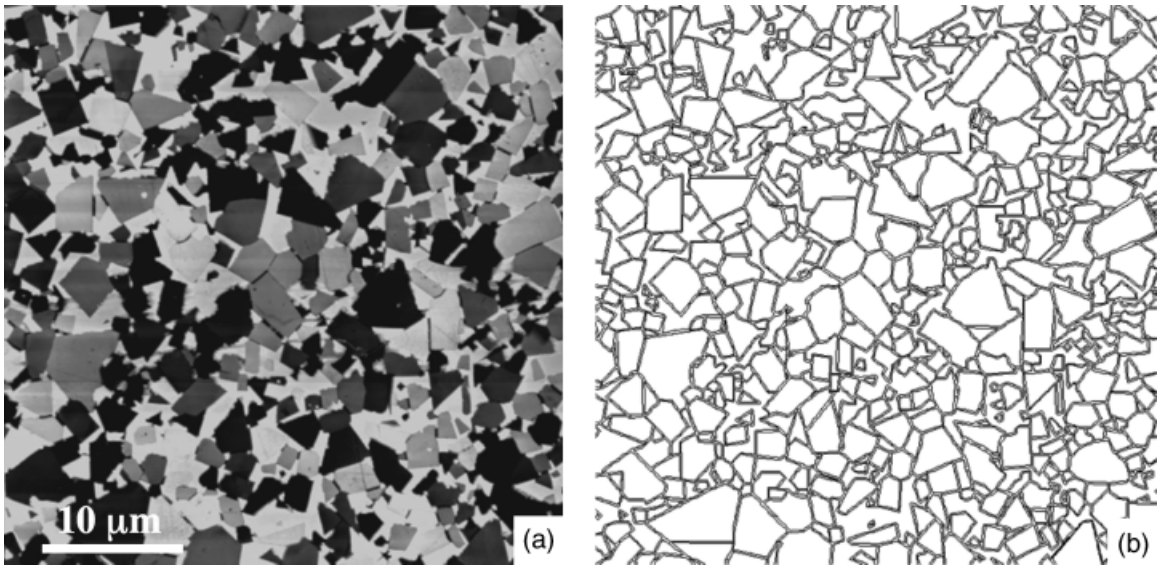

Fig. 1. (a) Contact atomic force microscopy (AFM) image of sample D. The lightest contrast corresponds to Co and the carbide crystals are a variety of darker shades. (b) A skeletonized map determined from the AFM image by tracing the boundary positions.

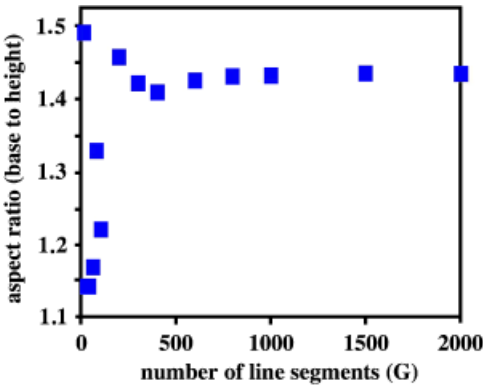

Fig. 2. Base-to-height aspect ratio of WC crystals in specimen G, determined from different numbers of observations.

grain size, L^*, is

$$L^* = \frac{2f_c}{2N_{cc} + N_{bc}} \quad (2)$$

(4) EBSD Mapping

Orientation maps were measured using an orientation imaging microscopy (OIM) system (TexSEM Laboratories Inc., Mahwah, NJ) incorporated in a Phillips XL40 FEG scanning electron microscope (SEM). Carbide grain orientation maps were recorded in the same areas that were imaged by AFM. Orientation measurements were made at intervals of 1.0 μm (A), 0.2 μm (B–E), and 0.4 μm (F and G) over total areas of 600 μm × 600 μm, 180 μm × 180 μm, and 360 μm × 360 μm, respectively. All OIM images were recorded at a specimen tilt of 70°, an accelerating voltage of 20 kV, and a spot size of 5.

The orientation maps, which contained only the carbide grain orientations, were processed so that both the WC/WC and WC/Co interface line segments could be extracted. The procedure for doing this has already been described in detail for the case of a $SrTiO_3/TiO_2$ composite.[12] The procedure here was identical, with WC being analogous to $SrTiO_3$.

(5) Analysis of Interface Distributions

The relative areas of the different types of interfaces were determined by previously described stereological techniques.[13,14] The observations needed for the stereological analysis are line segments, in the sample reference frame, that are associated with the crystal orientations. These segments were extracted from the orientation maps either by hand tracing or using the OIM software.[12] From these data, several related quantities can be derived. The simplest quantity to derive is the interface plane distribution (IPD). The IPD, λ(n), can be measured for the WC/Co interfaces or for the WC/WC grain boundaries. The IPD has two parameters that specify the interface normal orientation and, using our discretization scheme, there are a maximum of 324 distinguishable interface orientations. The symmetry operators of the hexagonal system apply to the IPD and this reduces the number of distinguishable interfaces by a factor of 12.

To determine the numbers of independent observations needed for a reliable IPD, we used the stereological method described in Saylor and Rohrer[13] to calculate the aspect ratio of WC crystals in specimen G using differing amounts of data. In this case, the aspect ratio refers to the ratio of the length along the edge of the (0001) basal facet of a trigonal pyramid to its height along a $(10\bar{1}0)$facet. The aspect ratio as a function of the number of observed line segments is illustrated in Fig. 2. It is clear that after approximately 500 observed line segments, the result is not affected by additional data. This provides an estimate of the number of line segments that are required for an accurate IPD of a hexagonal material. The IPDs presented here are based on substantially larger data sets.

The GBCD, λ(Δg, n), is a five-dimensional quantity that is sensitive to both the misorientation between WC grains, Δg, and the grain boundary plane orientation, n. If the GBCD is known, it is possible to plot the distribution of grain boundary planes at a fixed misorientation type. Using a resolution of 10° and our conventional discretization system, there are approximately 2.6×10^4 distinguishable grain boundaries in hexagonal polycrystals.[10] Therefore, evaluation of the GBCD requires many more observations than the IPD.

III. Results

(1) Geometric Characteristics

The effective particle diameter (L) and the mean intercept lengths (L^*) for a given sample are similar (see Table I). These differences result from the difference between the assumed circular shape and the actual polygonal shape of the carbide grains. The shape factors for trigonal prisms are not known, but for oblate ellipsoids of similar aspect ratios, the mean intercept lengths are expected to be from 0% to 3% smaller than the equivalent circle diameters.[15] The data are consistent with this range of values. A typical grain size distribution (for sample F) is shown in Fig. 3(a). This distribution is characteristic of all the samples studied and, to a good approximation, the logarithm of the grain diameters fits a normal distribution. The scale invariance of the distribution is illustrated in Fig. 3(b), which shows that the width of the normal distribution increases linearly with the grain size.

Figure 4(a) shows that the contiguity is approximately linear with the carbide volume fraction over the range of compositions

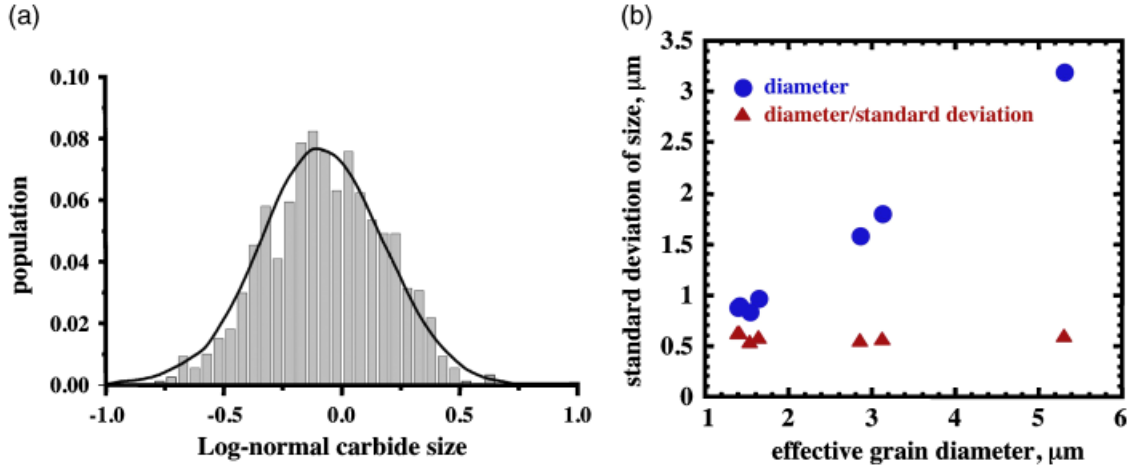

Fig. 3. (a) Grain size distribution in sample F. (b) Relationship between the mean grain diameter and standard deviation of the distribution of grain sizes for all specimens.

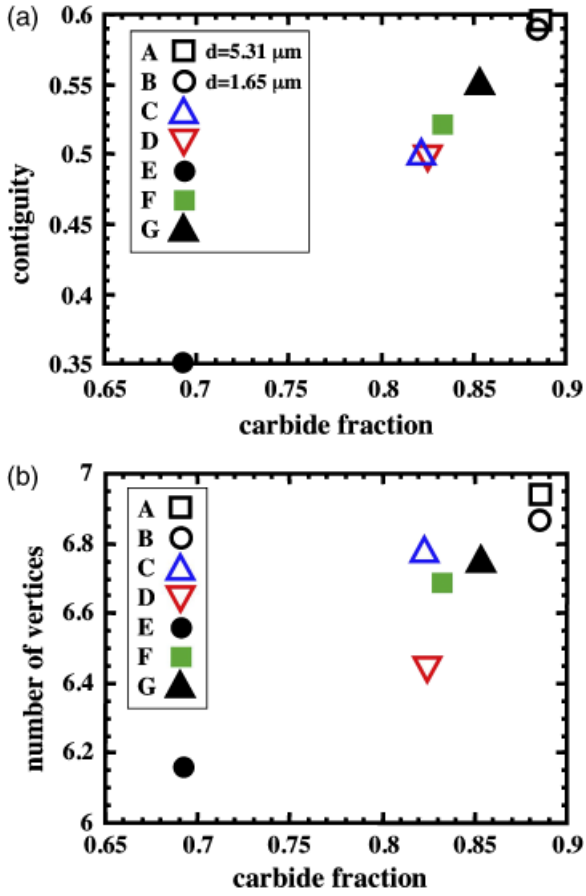

Fig. 4. (a) WC contiguity as a function of carbide volume fraction for all seven specimens. (b) The average number of WC vertices varies as a function of carbide volume fraction.

examined. More comprehensive studies, over a wider range of composition, have found that the contiguity increase is nonlinear.[16] Considering the scope of the present study, the current data are not inconsistent with accepted relationships between contiguity and binder volume fraction. Figure 4(a) contains evidence that the carbide volume fraction/contiguity relationship is also scale invariant in the range of specimens studied: samples A and B have very different grain sizes, but nearly the same carbide volume fractions and contiguity.[17] The average number

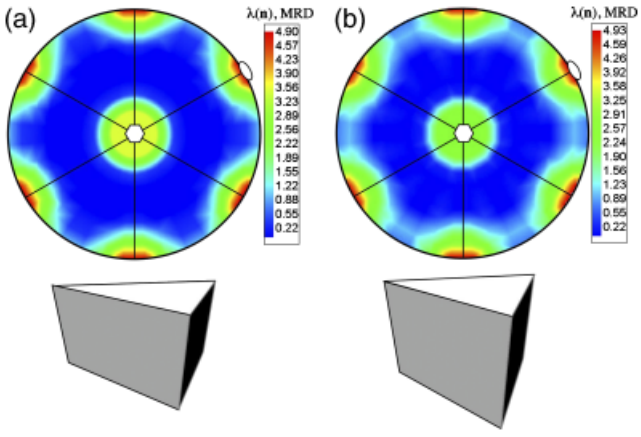

Fig. 5. Distribution of WC/Co interfaces in sample B (a) and sample E (b). Sample B has an average grain size of 1.58 μm and a carbide volume fraction of 0.88. Sample E has an average grain size of 1.40 μm and a carbide volume fraction of 0.69. The stereograms show peaks at the positions of the basal and prismatic facets, which are indicated by hexagons and ovals. Idealized polygons, based on these data, are shown below the stereograms.

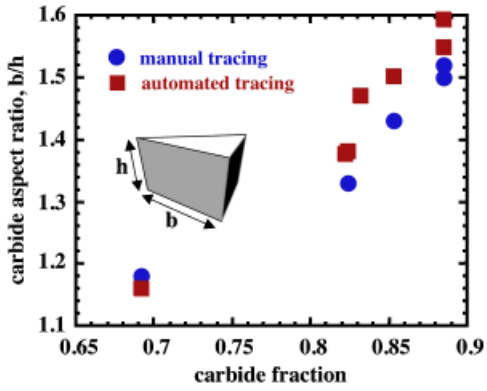

Fig. 6. Average base-to-height aspect ratios for the carbide grains in the seven samples, plotted as a function of carbide volume fraction. Aspect ratios determined from manually traced line segments and automatically traced line segments show the trend that the average shape becomes more plate-like as the carbide volume fraction increase.

of WC vertices varies with the carbide volume fraction as shown in Fig. 4(b). The average number of vertices increases as the carbide volume fraction increases. Because the contiguity and impingement also increase with the carbide volume fraction, the crystals become more equiaxed and have more vertices.

(2) Interface Distributions

The distributions of WC/Co interfaces in two of the samples are shown in Fig. 5. The distributions are plotted in multiples of a random distribution (MRD) units. Values greater than one indicate orientations that have areas greater than that expected in a random distribution, and values less than one indicate orientations that have areas less than that expected. In these stereograms, the basal orientation is in the center, marked by a hexagon, and the prismatic orientation is on the periphery, marked by an oval. The peaks in the distributions are at the (0001) (basal) and $(10\bar{1}0)$ (prismatic) positions, indicating that these are the most common surfaces. The maxima at these two orientations are common features of the interface plane distribution for all the samples. These results, combined with observations of crystal shapes on planes sections, have in the past been argued to show that, on average, the carbide crystals have a trigonal prismatic shape.[6]

Although the peaks at the prismatic orientation have approximately the same value in Fig. 5(a) and (b), the peaks at the basal position differ. The smaller relative peak at the basal orientation for sample E indicates that basal orientation makes up a smaller fraction of the total bounding surface. To quantify this difference, the line segments that give rise to these peaks can be used to evaluate the relative areas using a previously described procedure.[13] The relative areas are represented by the polygons below the stereogram with aspect (base-to-height) ratios of 1.5 (sample B) and 1.18 (sample E).

Changes in the average aspect ratio were found to be dependent upon the carbide volume fraction, as illustrated in Fig. 6. The trend in these data indicates that as the carbide volume fraction increases, the carbide grains become slightly more plate-like. Note that Fig. 6 shows average aspect ratios determined from both manually traced line segments and automatically traced line segments. The differences between the two methods are small and both show the same trend. It should be pointed out that samples with different amounts of Co were sintered at different temperatures. If the energy anisotropy is strongly influenced by temperature, then this may account for the changes in shape. While this cannot be ruled out, it is also true that samples with higher carbide contents were sintered at higher temperatures and have more anisotropic shapes. Because increasing the temperature usually decreases the surface energy anisotropy, temperature does not appear to be playing a dominant role in determining the shape variation.

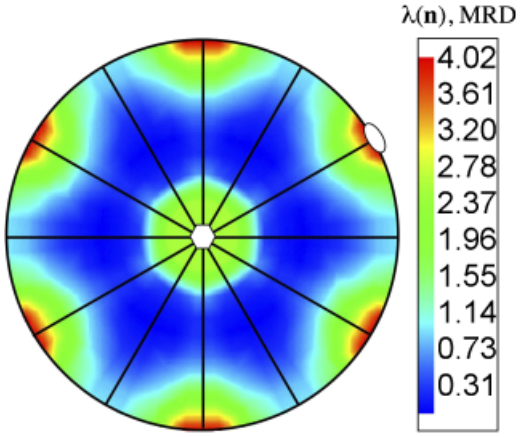

Fig. 7. Distribution of WC/WC grain boundary orientations, for all misorientations, in sample B. The distribution peaks at the positions of the basal and prismatic facets, which are indicated by a hexagon and oval.

The distributions of WC/WC grain boundary plane orientations were also calculated and an example (for sample B) is illustrated in Fig. 7. In this distribution of grain boundary plane orientations (averaged over all misorientations), we see that the most common orientations are $(10\bar{1}0)$ and (0001). This example is characteristic of all the other distributions. In comparison to the WC/Co IPD distributions in Fig. 5, the peaks at the basal and prismatic orientations are not as large, indicating that fewer of the grain boundaries have low index orientations than the phase boundaries. Using a 5° tolerance angle, approximately 80% of the WC/Co boundaries can be classified as basal or prismatic. Using the same criterion for the grain boundaries, only about 60% of the orientations can be classified as basal or prismatic. The ratios of basal grain boundary area to prismatic grain boundary area have also been calculated. In all samples it varies from 1.12 to 1.19 and there is no detectable trend with grain size or carbide volume fraction.

The distribution of WC/WC grain boundary misorientations was also studied in each sample. To a good approximation, the MDFs of the samples did not differ from the MDF presented in our earlier publication in which preliminary results from specimens A and E were presented.[6] The MDFs all exhibit a maximum for 90° rotations about the $[10\bar{1}0]$ axis. The next largest peak is for 30° rotations about the [0001] axis, and a smaller peak is found for 90° rotations around $[2\bar{1}\bar{1}0]$. A preliminary analysis of the habit planes for the $90°/[10\bar{1}0]$ boundary indicated that these are nearly all twist boundaries and an analysis of the $30°/[0001]$ boundaries indicated that these were a combination of twist boundaries and asymmetric tilt boundaries on $[10\bar{1}0]$ and $[10\bar{1}0]$ planes.[6] By counting all boundaries whose axis and angle parameters are within 3° of the ideal, and whose boundary traces are within 5° of the ideal boundary plane, we find that the $90°/[10\bar{1}0]$ boundaries make up 11%–14% of the populations in each of the samples and the $30°/(0001)$ boundaries make up 2%–3% of the populations. Variations within these limits do not correlate with carbide volume fraction or grain size.

The similarity of the misorientation distributions, the grain boundary plane distributions, and the basal-to-prismatic area ratios of the eight specimens suggest that all have very similar grain boundary character distributions. While none of the data sets together have enough information for a complete calculation of the five-parameter GBCD, the combination of all of the similar data sets comprises approximately 2.5×10^5 line segments. As this is nearly ten times the number of distinct interfaces, we have a sufficient number of observations to calculate the distribution of grain boundary planes at the most common points in misorientation space, which make up a disproportionately large subset of the data. The plane distributions for the $90°/[10\bar{1}0]$, $30°/[0001]$, and $90°/[\bar{2}110]$ grain boundaries are shown in Fig. 8.

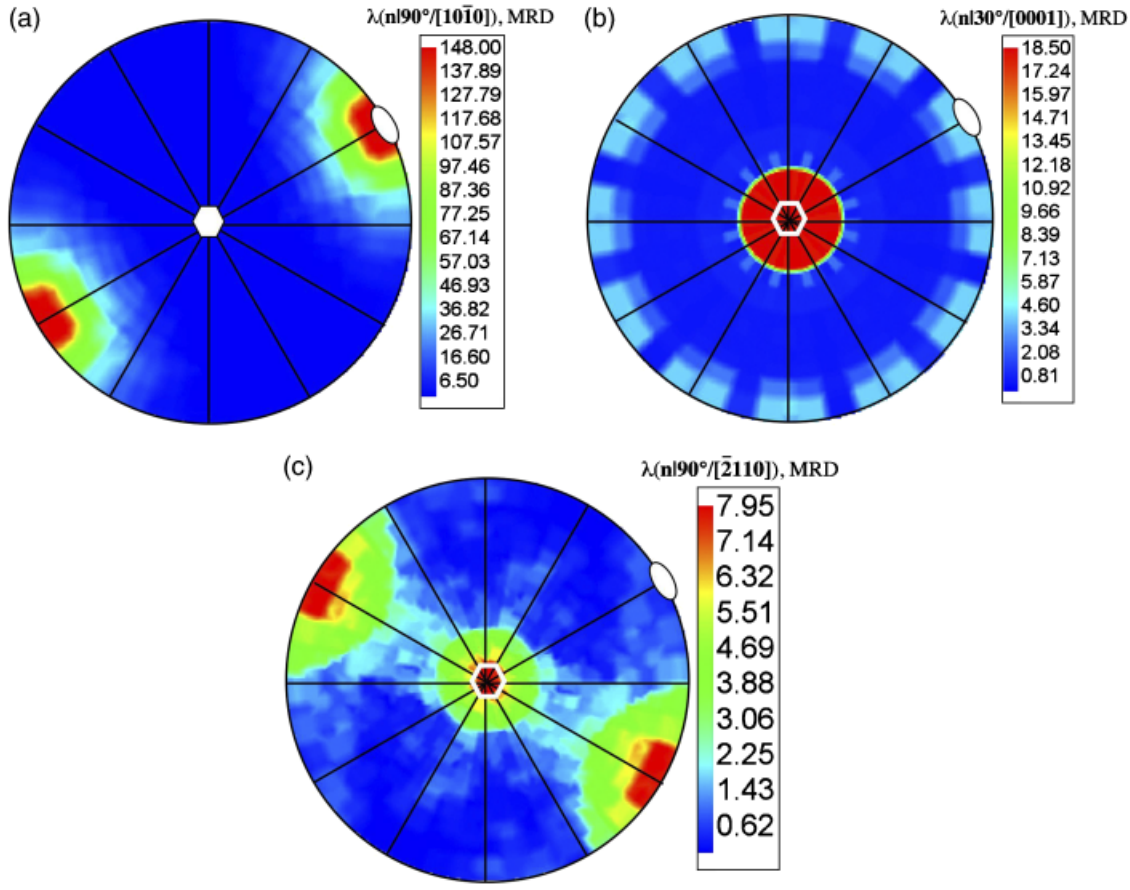

Fig. 8. Grain boundary plane distributions in WC, for (a) the $90°/[10\bar{1}0]$ grain boundary, (b) the $30°/(0001)$, and (c) the $90°/[\bar{2}110]$ grain boundary.

The grain boundary plane distributions for the three most common grain boundaries show a strong preference for planes with special geometries. For example, for the $90°/[10\bar{1}0]$ grain boundary, the planes have $(10\bar{1}0)$ orientations, meaning that these are pure twist grain boundaries. The peak at (0001) for the $30°/[0001]$ grain boundary also corresponds to a pure twist grain boundary; the smaller peaks at the prismatic positions correspond to asymmetric grain boundaries bounded on one side by a $(\bar{2}110)$ plane and on the other by a $(10\bar{1}0)$ plane. Finally, the $90°/[\bar{2}110]$ grain boundaries are asymmetric, bounded on one side by (0001) and on the other by $(10\bar{1}0)$. It is clear from these observations that the most common grain boundaries favor low index habit planes.

IV. Discussion

The results presented here indicate that in a range of different WC–Co composites, the concentration of special boundaries is constant. Kumar et al.[9] recently reported that the concentration of $90°/[10\bar{1}0]$ grain boundaries decreased as the grain size increased. However, in these studies, the GBCD was monitored from the earliest stages of processing, from grain sizes of 1.1–1.7 μm. In contrast, samples with the smallest grain sizes considered here are best compared with the final stage of their experiment, where the length fraction of $90°/[10\bar{1}0]$ grain boundaries is decreasing slowly, if at all. Therefore, there might be an initial change in the concentration of these boundaries that depends on the starting materials, but by the time the grain size is greater than 1.5 μm, the concentration is roughly constant. This idea is consistent with the TEM observation that many $90°/[10\bar{1}0]$ grain boundaries exist in submicrometer WC powders before consolidation.[5] Furthermore, liquid-phase sintering studies indicate that these boundaries can be preserved during growth.[8] In other words, it is possible that the initial concentration of these boundaries is greater than the equilibrium value and that the concentration decreases to equilibrium during growth.

The present observations suggest that a steady-state distribution of grain boundary types occurs in these materials. Prior studies of grain boundary character distributions in single-phase polycrystals have indicated that grain boundary character distributions are inversely related to grain boundary energy.[10] These observations have been supported by grain growth simulations that have shown that steady-state characteristic GBCDs develop in the early stages of growth.[18–20] More recently, a mechanistic model for the development of steady-state GBCDs has been formulated.[21] In this model, the energy of a boundary determines its relative area and its area affects the rate at which it is eliminated during the growth in such a way that low energy, large-area grain boundaries accumulate in the system until a steady state is reached. Based on the consistency of the GBCDs reported here, we conclude that the WC grain boundary populations have reached a steady state that is determined by the relative grain boundary energies. While the energies of some WC grain boundaries have been calculated, the available data are not comprehensive enough to support a comparison with the GBCD results.[7,22–24]

To determine the influence of geometrically and energetically special grain boundaries on the mechanical properties of these materials, it will be necessary to vary the concentration, while maintaining approximately the same grain size and Co binder fraction. Because the GBCD depends on the grain boundary energy, and the energies of grain boundaries can be altered by segregated impurities, doping is one possible route that might be used to control the populations of special grain boundaries. In fact, in a recent comparative study of TiO_2 and Nb-doped TiO_2, it was shown that doping influenced the GBCD by changing the energies and populations of boundaries so that the populations of low energy boundaries were enhanced with respect to higher energy boundaries.[25] Of course, it must also be noted that impurities themselves can influence mechanical properties in ways that are difficult to predict.

V. Conclusions

WC–Co interfaces and WC/WC grain boundaries strongly favor low index interface planes. While carbide grain shape varies with Co content, it is independent of grain size. Of all the WC grain boundaries, the most common are the $90°/[10\bar{1}0]$twist boundaries, the $30°/(0001)$ twist boundaries, and the asymmetric $90°/[\bar{2}110]$ boundaries. The boundary populations do not vary with grain size or carbide volume fraction, suggesting that they are determined by the relative energies of the interfaces and not by kinetic processes.

References

[1]J. Gurland, "New Scientific Approaches to the Development of Tool Materials," *Int. Mater. Rev.*, **33** [3] 151–66 (1988).

[2]X. Deng, B. R. Patterson, K. K. Chawla, M. C. Koopman, C. Mackin, Z. Fang Z, G. Lockwood, and A. Griffo, "Microstructure/Hardness Relationship in a Dual Composite," *J. Mater. Sci. Lett.*, **21** [9] 707–9 (2002).

[3]X. Deng, B. R. Patterson, K. K. Chawla, M. C. Koopman, Z Z. Fang, G. Lockwood, and A. Griffo, "Mechanical Properties of a Hybrid Cemented Carbide Composite," *Int. J. Ref. Metals Hard. Mater.*, **19** [4–6] 547–52 (2001).

[4]V. Randle, "Twinning-Related Grain Boundary Engineering," *Acta Mater.*, **52** [14] 4067–81 (2004).

[5]S. Lay and M. Loubradou, "Characteristics and Origin of Clusters in Submicron WC–Co Cermets," *Phil. Mag.*, **83** [23] 2669–79 (2003).

[6]C.-S. Kim and G. S. Rohrer, "Geometric and Crystallographic Characterization of WC Surfaces and Grain Boundaries in WC–Co Composites," *Interface Sci.*, **12** [1] 19–27 (2004).

[7]M. Christensen and G. Wahnström, "Effects of Cobalt Intergranular Segregation on Interface Energetics in WC–Co," *Acta Mater.*, **52** [8] 2199–207 (2004).

[8]J.-D. Kim, S. J. Kang, and J.-W. Lee, "Formation of Grain Boundaries in Liquid Phase Sintered WC–Co Alloys," *J. Am. Ceram. Soc.*, **88** [2] 500–3 (2005).

[9]V. Kumar, Z. Z. Fang, S. I. Wright, and M. M. Nowell, "An Analysis of Grain Boundaries and Grain Growth in Cemented Tungsten Carbide using Orientation Imaging Microscopy," *Metall. Mater. Trans. A*, **37A** [3] 599–607 (2006).

[10]G. S. Rohrer, D. M. Saylor, B. S. El-Dasher, B. L. Adams, A. D. Rollett, and P. Wynblatt, "The Distribution of Internal Interfaces in Polycrystals," *Zeitschrift fur Metallkunde*, **95** [4] 197–214 (2004).

[11]B. Roebuck, E. A. Almond, and A. M. Cottenden, "The influence of Composition, Phase Transformation and Varying the Relative F.C.C. and H.C.P Phase Contents on the Properties of Dilute Co–W–C Alloys," *Mater. Sci. Eng.*, **66** [2] 179–94 (1984).

[12]T. Sano and G. S. Rohrer, "Experimental Evidence for the Development of Bimodal Grain Size Distributions by the Nucleation-Limited Coarsening Mechanism," *J. Am. Ceram. Soc.*, **90** [1] 211–6 (2007).

[13]D. M. Saylor and G. S. Rohrer, "Determining Crystal Habits from Observations of Planar Sections," *J. Am. Ceram. Soc.*, **85** [11] 2799–804 (2002).

[14]D. M. Saylor, B. S. El-Dasher, B. L. Adams, and G. S. Rohrer, "Measuring the Five Parameter Grain Boundary Distribution From Observations of Planar Sections," *Metall. Mater. Trans.*, **35A** [7] 1981–9 (2004).

[15]J. C. Russ, *Practical Stereology*, pp. 57–9. Plenum Press, New York, 1986.

[16]R. M. German, "The Contiguity of Liquid Phase Sintered Microstructures," *Metals Trans. A*, **16** [7] 1247–52 (1985).

[17]S. Luyckx and A. Love, "The Dependence of the Contiguity of WC on Co Content and its Independence from WC Grain Size in WC–Co Alloys," *Int. J. Ref. Metals Hard. Mater.*, **24** [1–2] 75–9 (2006).

[18]E. A. Holm, G. N. Hassold, and M. A. Miodownik, "On Misorientation Distribution Evolution During Anisotropic Grain Growth," *Acta Mater.*, **49** [15] 2981–91 (2001).

[19]M. Upmanyu, G. N. Hassold, A Kazaryan, E. A. Holm, Y. Wang, B. Patton, and D. J. Srolovitz, "Boundary Mobility and Energy Anisotropy Effects on Microstructural Evolution During Grain Growth," *Interface Sci.*, **10** [2–3] 201–16 (2002).

[20]J. Gruber, D. C. George, A. P. Kuprat, G. S. Rohrer, and A. D. Rollett, "Effect of Anisotropic Grain Boundary Properties on Grain Boundary Plane Distributions During Grain Growth," *Scr. Mater.*, **53** [3] 351–5 (2005).

[21]G. S. Rohrer, J. Gruber, and A. D. Rollett, "A Model for the Origin of Anisotropic Grain Boundary Character Distributions in Polycrystalline Materials," *Proceedings of the 15th International Conference on Texture of Materials*, Submitted, 2007.

[22]M. Christensen, S. V. Dudiy, and G. Wahnström, "First Principles Simulations of Metal–Ceramics Interface Adhesion: Co/WC versus Co/TiC," *Phys. Rev. B*, **65** [4] 045408 (2002).

[23]M. Christensen and G. Wahnström, "Co-phase Penetration of WC(10-10)/WC(10-10) Grain Boundaries from First Principles," *Phys. Rev. B*, **67** [11] 115415 (2003).

[24]M. Christensen and G. Wahnström, "Strength and Reinforcement of Interfaces in Cemented Carbides," *Int. J. Ref. Metals Hard. Mater.*, **24** [1–2] 80–8 (2006).

[25]Y. Pang and P. Wynblatt, "Effects of Nb Doping and Segregation on the Grain Boundary Plane Distribution in TiO_2," *J. Am. Ceram. Soc.*, **89** [2] 666–71 (2006). □